American Mineralogist, Volume 104, pages 1416–1420, 2019

Solubility behavior of δ-AlOOH and ε-FeOOH at high pressures

Chaowen Xu[1,*,†], Masayuki Nishi[1], and Toru Inoue[1,2,3]

[1]Geodynamics Research Center, Ehime University, 2-5 Bunkyo-cho, Matsuyama 790-8577, Japan
[2]Department of Earth and Planetary Systems Science, Hiroshima University, 1-3-1 Kagamiyama, Higashi-Hiroshima 739-8526, Japan.
Orcid 0000-0002-5044-6479
[3]Hiroshima Institute of Plate Convergence Region Research (HiPeR), Hiroshima University, Higashi-Hiroshima, Hiroshima 739-8526, Japan

Abstract

Low-pressure polymorphs of AlOOH and FeOOH are common natural oxyhydroxides at the Earth's surface, which may transport hydrogen to the deep mantle via subduction. At elevated pressures, the low-pressure polymorphs transform into δ-AlOOH and ε-FeOOH with $CaCl_2$-type structure, which form a solid solution above 18 GPa. Nevertheless, few studies have examined the solid solution behavior of this binary system in detail. In this study, we ascertain the phase relations in the AlOOH–FeOOH binary system at 15–25 GPa and 700–1200 °C. X-ray diffraction (XRD) measurements of quenched samples show that δ-AlOOH and ε-FeOOH partly form solid solutions over wide pressure and temperature ranges. Our results demonstrate that a binary eutectic diagram is formed without dehydration or melting below 1200 °C at 20 GPa. We also observe that the maximum solubilities of Al and Fe in the solid solutions are more strongly influenced by temperature than pressure. Our results suggest that the $CaCl_2$-type hydroxides subducted into the deep mantle form a solid solution over a wide composition range. As AlOOH and FeOOH are present in hydrous crust, these phases may be subducted into the deep interior, transporting a significant amount of hydrogen to deeper regions. Therefore, a better understanding of this binary system may help elucidate the model geodynamic processes associated with the deep water cycling in the Earth.

Keywords: Solubility behavior, δ-AlOOH, ε-FeOOH, high pressures; Physics and Chemistry of Earth's Deep Mantle and Core

Introduction

H_2O, which is present as H^+ or OH^- in minerals, plays an important role in geological processes in the Earth's interior, affecting the physical and chemical properties of its surroundings such as melting temperature, melt composition, and phase relations (e.g., Inoue 1994; Chang et al. 2017; Hwang et al. 2017; Myhill et al. 2017). Water may be transported into the deep Earth via subducting slabs within hydrous phase. Previous studies have been evaluated the stability regions of various hydrous phases, especially dense hydrous magnesium silicates (DHMSs), which have been suggested as potential water carriers to the transition zone and even to the lower mantle in cold subducting slabs (e.g., Frost and Fei 1998; Litasov and Ohtani 2003; Komabayashi et al. 2005).

The oxyhydroxides goethite (α-FeOOH) and AlOOH are common hydrous minerals in the sediments. δ-AlOOH is a high-pressure polymorph of diaspore (α-AlOOH) and boehmite (γ-AlOOH) (e.g., Suzuki et al. 2000; Xue and Kanzaki 2007) that has been shown to be stable up to 170 GPa (e.g., Sano et al. 2008; Tsuchiya and Tsuchiya 2011; Ohira et al. 2014). The other potential water carrier, ε-FeOOH, which is a high-pressure polymorph of goethite (α-FeOOH), akaganeite (β-FeOOH), and lepidocrocite (γ-FeOOH), has a $CaCl_2$-type structure as δ-AlOOH (e.g., Suzuki 2010). ε-FeOOH has been known to have a stability field in the lower mantle (e.g., Nishi et al. 2017). To investigate the physical properties of these $CaCl_2$-type hydrous phases, numerous experiments and calculations have been performed particularly addressing the stability, compressibility, and crystallography of the end-members δ-AlOOH, ε-FeOOH, and phase H ($MgSiO_4H_2$) (e.g., Tsuchiya et al. 2002; Panero and Stixrude 2004; Xue and Kanzaki 2007; Suzuki 2010; Komatsu et al. 2011; Kuribayashi et al. 2013; Nishi et al. 2014; Bindi et al. 2014; Zhong et al. 2016; Thompson et al. 2017). Earlier results have also shown that phase H and δ-AlOOH form a solid solution because of their similar structures (e.g., Ohira et al. 2014; Panero and Caracas 2017). This AlOOH-$MgSiO_4H_2$ solid solution can coexist with bridgmanite above 40 GPa along the slab geotherm (e.g., Nishi et al. 2014; Ohira et al. 2014; Nishi 2015; Bindi et al. 2015; Walter et al. 2015; Panero and Caracas 2017).

The discovery of hydrous aluminum silicate phase Egg ($AlSiO_3OH$) as inclusions in diamond implies that the crustal hydrous material may have been subducted into the transition zone, at least locally (e.g., Wirth et al. 2007). More recently, hydrous ringwoodite and ice-VII were also found as inclusions in diamond, suggesting their presence in a partially hydrated mantle transition zone and the lower mantle (e.g., Pearson et al. 2014; Tschauner et al. 2018). Because AlOOH and FeOOH are common oxyhydroxides at Earth's surface, these solid solutions in the deep Earth play an important role for water transportation

* E-mail: dkchaowen@126.com

† Special collection papers can be found online at http://www.minsocam.org/MSA/AmMin/special-collections.html.

0003-004X/19/0009–1416$05.00/DOI: https://doi.org/10.2138/am-2019-7064

in subducted slabs (e.g., Nishi et al. 2017). Nevertheless, the solubility behavior of this binary system is not well constrained. A better understanding of this system will also help elucidate the water cycle of iron-rich martian mantle. Therefore, this study was conducted to determine the solubility behavior of AlOOH-FeOOH binary system at 15–25 GPa and 700–1200 °C.

Experimental methods

We conducted high-pressure high-temperature experiments using a Kawai-type 1000-ton multi-anvil apparatus at the Geodynamics Research Center (GRC), Ehime University. Pressures were calibrated at room temperature by diagnostic changes in the electrical resistances of ZnTe (9.6 and 12.0 GPa), ZnS (15.5 GPa), GaAs (18.3 GPa), and GaP (23.0 GPa) induced by the semiconductor–metal phase transitions at high pressures. Tungsten carbide cubes with a truncation edge length (TEL) of 4 mm were used in combination with Co-doped MgO-octahedra of 10 mm edge length (10/4 assemblage). Preformed pyrophyllite gaskets were used between the cubes, $LaCrO_3$ was used as the heater, and a gold sample capsule was used in the cell assemblage. The temperature was monitored using a $W_{97}Re_3$-$W_{75}Re_{25}$ thermocouple, and the electromotive force (EMF) was not corrected for the effects of pressure. The sample was compressed to a desired pressure and then the oil pressure was held constant. Subsequently, the AC power was supplied to the heater in the furnace assemblage. After heating at high pressure, the power was stopped by shutting off the electric power supply. Samples were recovered after releasing pressure slowly for 12 h.

The starting material, with a chemical composition of $(Al_{0.5}Fe_{0.5})OOH$, was prepared by mixing oxides $Al(OH)_3$, Al_2O_3, and Fe_2O_3 in appropriate proportions. The recovered run products were mounted in epoxy resin and were polished to perform phase identification and chemical composition analysis. The phase assemblages were characterized using a micro-focus X-ray diffractometer (MicroMax-007HF; Rigaku Corp.) with Cu*K*α radiation. The obtained data were processed by 2PD software, which can display and process two-dimensional data, including smoothing, background correction and 2D to 1D conversion. The micro-textures and composition were obtained using a field emission scanning electron microscope (FESEM, JSM7000F; JEOL) combined with an energy-dispersive X-ray spectrometer (EDS, X-MaxN; Oxford Instruments). Working parameters of 15 kV, 1 nA and collection times of 30–50 s were used. The chemical composition was analyzed using EDS. We used software (Aztec ver. 2.4; Oxford Instruments Nanotechnology Tools Ltd.) to process EDS data. Stoichiometric composition of $(Fe_X,Al_{1-X})OOH$ was assumed, where X is the Fe/(Fe+Al) ratio. The total contents of the obtained $(Fe_X,Al_{1-X})OOH$ are approximately 85 wt%.

Results and discussion

Table 1 presents the experimental conditions and chemical compositions of the synthesized samples determined by EDS. In all runs, the backscattered electron (BSE) images show that the recovered samples consist mainly of two phases except for the highest temperature run (1200 °C), which was likely above the solidus (Fig. 1). X-ray diffraction (XRD) patterns of the samples indicate that these phases are ε-FeOOH and δ-AlOOH (Fig. 2), although their peak positions are shifted from those of the ideal end-members, as discussed later.

At 20 GPa and 900 °C, a BSE image (Fig. 1a) shows the presence of two phases in bright and dark regions with respective chemical compositions of ε-$Fe_{0.78}Al_{0.22}OOH$ and δ-$Al_{0.91}Fe_{0.09}OOH$. These chemical compositions can be explained to be the result of forming solid solutions because of the similar crystal structures of the two end-members. The compositions and grain sizes of both phases changed at elevated temperatures up to 1100 °C (Fig. 1b). With increasing temperature, the Al/Fe ratio decreases in Al-rich δ-phase, whereas it increases in Fe-rich ε-phase (Table 1). At 1200 °C, Al-rich δ-phase was found to coexist with iron oxide (bright regions) and melt (Fig. 1c), which means Fe-rich ε-phase totally decomposed at this condition. Some amount of H_2O escaped when the capsule was opened. At a lower pressure of 15 GPa at 1000 °C, the crystal shape of Al-rich δ-phase seemed to transform into an elongated shape (Fig. 1d), which might occur because of the phase change, as indicated by XRD (described below).

Selected room-temperature XRD patterns of the recovered samples are summarized in Figure 2. Al-rich δ-phase, Fe-rich ε-phase and low-pressure Al-rich α-phase are observed. All the peaks are consistent with the earlier studies of δ-AlOOH and ε-FeOOH (e.g., Suzuki et al. 2000; Suzuki 2010; Kuduvalli et al. 2008; Mashino et al. 2016). Our results suggest that the solid solutions are formed in the δ-AlOOH–ε-FeOOH binary systems over large compositional ranges. The XRD peaks of Fe-rich ε-phase and Al-rich δ-phase are shifted to toward higher and lower angles, respectively, at 1100 °C and 20 GPa compared to 900 °C and 20 GPa. These observations are consistent with SEM-EDS results, which indicate that Al contents increase in Fe-rich ε-phase, whereas Fe contents increase in Al-rich δ-phase at higher temperatures (Table 1). At 15 GPa and 1000 °C, probably because of the low pressure, a diffraction peak of α-AlOOH instead of δ-AlOOH is present (Fig. 2c).

Figure 3 plots the unit-cell volumes of solid solutions between δ-AlOOH and ε-FeOOH as a function of FeOOH content. As shown in this figure, partial solid solutions were formed at 20–25 GPa and 700–1200 °C. The volume of Fe-rich ε-phase increases with increasing the Fe content, likely because of the large size of $^{VI}Fe^{3+}$ ion (0.645 Å) relative to $^{VI}Al^{3+}$ ion (0.535 Å).

Table 1. Experiment run conditions and mineral compositions of recovered samples in the AlOOH-FeOOH binary system

P (GPa)	*T* (°C)	Duration time (min)	EDS analysis number	Phase	Al_2O_3	Fe_2O_3	Total
15	1000	60	27	α-$Al_{0.92}Fe_{0.08}OOH$	71.71(200)	10.33(98)	82.04(178)
				ε-$Fe_{0.75}Al_{0.25}OOH$	14.39(89)	67.83(90)	82.22(109)
20	700[a]	60	29	δ-$Al_{0.93}Fe_{0.07}OOH$	70.82(169)	11.50(62)	82.32(136)
				ε-$Fe_{0.76}Al_{0.24}OOH$	14.29(154)	69.20(155)	83.49(74)
20	900	60	32	δ-$Al_{0.90}Fe_{0.10}OOH$	72.21(81)	12.06(84)	84.27(84)
				ε-$Fe_{0.78}Al_{0.22}OOH$	12.67(113)	69.41(97)	82.08(43)
20	1000	60	35	δ-$Al_{0.81}Fe_{0.19}$ OOH	60.59(107)	22.51(73)	83.10(180)
				ε-$Fe_{0.64}Al_{0.36}OOH$	22.27(74)	62.00(81)	84.27(57)
20	1100	40	32	δ-$Al_{0.78}Fe_{0.22}$ OOH	58.89(128)	26.36(92)	85.25(80)
				ε-$Fe_{0.55}Al_{0.45}OOH$	28.62(125)	54.30(126)	82.92(56)
20	1200	40	25	δ-$Al_{0.72}Fe_{0.28}OOH$	53.48(158)	33.05(140)	86.53(50)
				Fe_2O_3	1.91(17)	98.39(48)	100.30(52)
25	1000	90	30	δ-$Al_{0.86}Fe_{0.14}OOH$	65.13(71)	17.27(52)	82.40(74)
				ε-$Fe_{0.70}Al_{0.30}OOH$	17.64(64)	64.66(63)	82.30(45)

Note: Values in parentheses denote measurement uncertainties.
[a] Chemical composition of the Fe-rich phase might have a large uncertainty because of the small crystals.

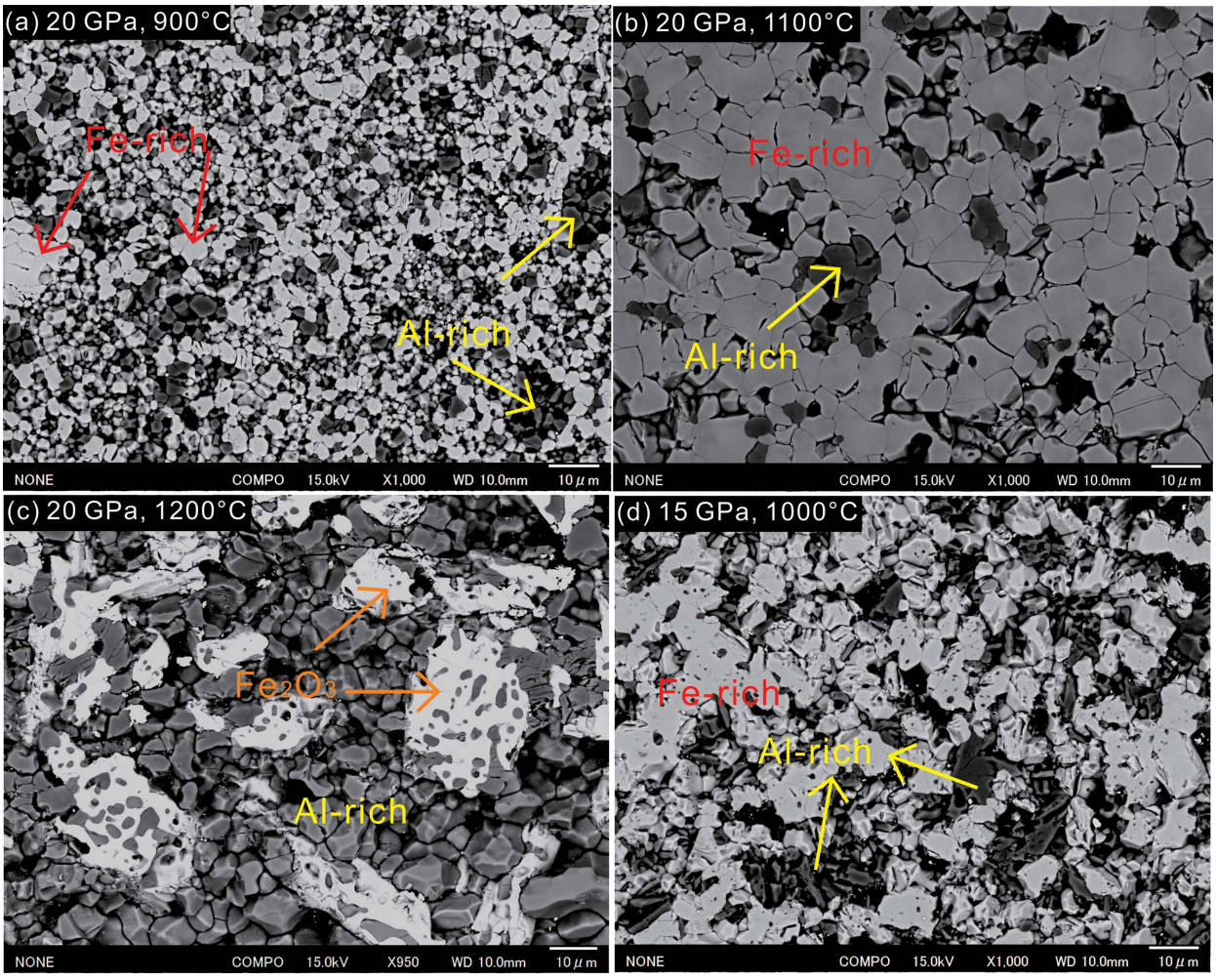

FIGURE 1. Backscattered electron images of representative run products under various pressure and temperature conditions. Al-rich: Al-rich phase, Fe-rich: Fe-rich phase. (**a**) 20 GPa, 900 °C; (**b**) 20 GPa, 1100 °C; (**c**) 20 GPa, 1200 °C; and (**d**) 15 GPa, 1000 °C. Some amount of H_2O escaped when the capsule was opened. (Color online.)

This is consistent with previous experimental studies of a similar (Al,Fe)OOH bulk composition conducted at 21 and 40 GPa (e.g., Fig. 4; Kawazoe et al. 2017; Nishi et al. 2017).

The phase relations of the δ-AlOOH–ε-FeOOH binary system are presented in Figure 4. The dashed line in Figure 4 shows the dehydration temperature of δ-AlOOH (approximately 1200 °C) at 20 GPa (e.g., Ohtani et al. 2001). Similar thermal stability limit for δ-AlOOH was also reported in the previous studies that show the decomposition of the phase Egg into δ-AlOOH + SiO_2 at ~1200 °C at transition-zone pressures (e.g., Sano et al. 2004; Fukuyama et al. 2017). In this study, a binary eutectic diagram is formed without dehydration or melting below the dashed line in Figure 4 from 700 to 1100 °C at 20 GPa, and at pressures of 15–25 GPa at 1000 °C (except for the stability field of α-AlOOH). AlOOH and FeOOH solid solutions are observed over wide temperature and pressure ranges. Although an earlier study described the dehydration of δ-AlOOH at 1200 °C (e.g., Ohtani et al. 2001), our data show that Al-rich δ-phase persists at 1200 °C, whereas the Fe-rich ε-phase decomposes into Fe_2O_3 + H_2O (Fig. 2d) under the same *P*–*T* conditions. Al-rich δ-phase was observed at 1200 °C in contrast to previous studies (e.g., Ohtani et al. 2001). This suggests that a thermal gradient may have existed in our cell but could not be conclusively identified, because we placed the thermocouple at the center of the heater, where the highest temperature should be expected. To the best of our knowledge, no previous study has determined the melting temperature of ε-FeOOH at the transition zone pressure conditions. Our results suggest that ε-FeOOH has a lower dehydration temperature than that of δ-AlOOH. We also found that the Al-content in FeOOH is larger than the Fe-content of AlOOH. Because of the smaller ionic radius of Al^{3+} than Fe^{3+}, on the other hand, Al^{3+} is more compatible with the octahedral site in ε-FeOOH than that of Fe^{3+} in δ-AlOOH, leading to the higher Al-content in ε-FeOOH than the Fe-content of δ-AlOOH. It should be pointed out that EDS cannot precisely measure chemical compostion of the recovered sample at 700 °C due to its small crystal size. Therefore, chemical compositions of the two phases at 700 °C (dashed circles in Fig. 4) were estimated from the relation between unit-cell volume and composition from Figure 3.

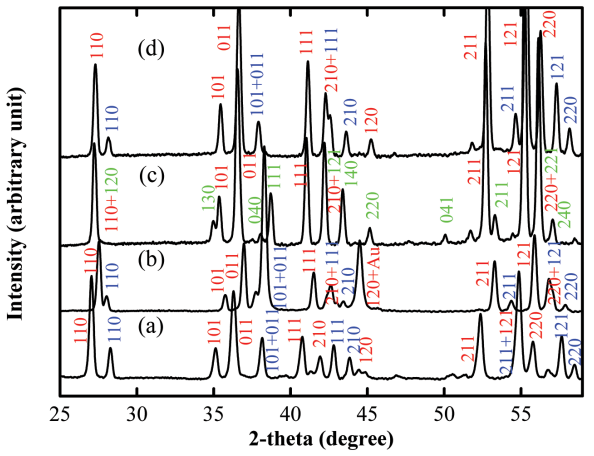

FIGURE 2. Selected XRD patterns of recovered run products: (**a**) 20 GPa, 900 °C; (**b**) 20 GPa, 1100 °C; (**c**) 15 GPa, 1000 °C; and (**d**) 25 GPa, 1000 °C. Index numbers in red and blue represent Fe-rich ε-FeOOH and Al-rich δ-AlOOH, respectively. At 15 GPa (**c**), α-AlOOH (green) appeared instead of δ-AlOOH. (Color online.)

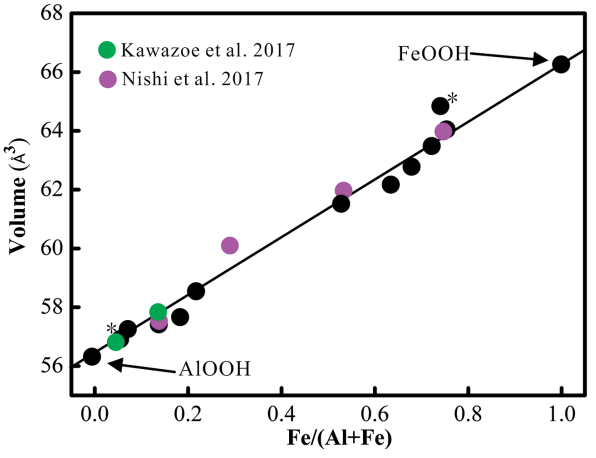

FIGURE 3. Cell volumes of intermediate compositions in the δ-AlOOH–ε-FeOOH binary system at ambient conditions as a function of ε-FeOOH content. All chemical compositions (including literature data) were determined using EDS, and the volumes were determined by XRD. The trend of our data is consistent with those reported for solid solutions in the (Al,Fe)OOH bulk composition at 21 and 40 GPa (green and pink color), which suggests that the solid solutions can be formed in a wide pressure range. An asterisk (*), denotes volume determined from the sample with a large uncertainty due to its small crystalline size. The error bars of the measured cell volumes are smaller than the symbol size. (Color online.)

The chemical compositions and their temperature dependences of δ-phase and ε-phase at 20 GPa in this work are consistent with those found at 40 GPa in an earlier study (e.g., Fig. 4; Nishi et a. 2017). Consequently, compared with pressure, temperature seems to play a more significant role in the partitioning of Al and Fe between δ-AlOOH and ε-FeOOH at pressures up to 40 GPa. For example, although the samples were recovered from different pressures, the similar Al/Fe ratios of hydroxides were observed at 1000 °C. This means that temperature has a more

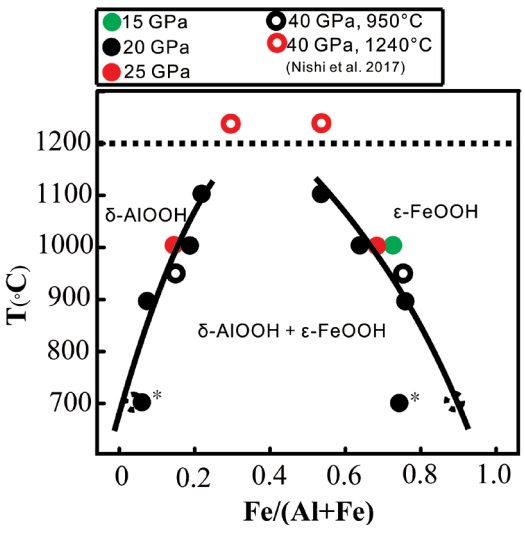

FIGURE 4. Phase relations in the δAlOOH-εFeOOH binary system at various pressures and temperatures as a function of ε-FeOOH content. Dashed circles denote the compositions at 700 °C, as estimated from the relation between unit-cell volume and composition shown in Figure 3. The dashed line shows the dehydration temperature of δ-AlOOH (ca. 1200 °C) at 20 GPa (e.g., Ohtani et al. 2001). A broad range of intermediate compositions in the FeOOH-AlOOH system were identified in the whole *P*–*T* range of 15–25 GPa and 700–1200 °C. Open circles show a solid solution between δ-AlOOH and ε-FeOOH synthesized at 40 GPa (e.g., Nishi et al. 2017), suggesting that pressure can increase the dehydration temperature. (Color online.)

profound influence on compositional stability than pressure in the AlOOH-FeOOH binary system. As a result, a series of intermediate compositions were identified in the temperature range 700–1250 °C. On the other hand, the dehydration temperatures of both δ-phase and ε-phase are likely to increase concomitantly with increasing pressure, because these phases were observed at 1240 °C and 40 GPa in an earlier study (Fig. 4). Therefore, AlOOH and FeOOH may form a complete solid solution near the solidus at higher pressures, although they do not at 20 GPa.

IMPLICATIONS

The $CaCl_2$-type FeOOH phase has been observed to remain stable at 76 GPa and 2150 K (e.g., Hu et al. 2016). The FeOOH and AlOOH end-members form solid solutions at elevated temperatures and pressures in the subducting plate. As such, they are expected to transport water (H^+) into the deep lower mantle, even undergoing change in their respective chemical compositions depending on the temperature, as shown in this study. Moreover, δ-AlOOH reportedly forms a solid solution with phase H ($MgSiO_4H_2$) and coexists with bridgmanite along the pressure and temperature path corresponding to the subduction (e.g., Nishi et al. 2014; Ohira et al. 2014; Panero and Caracas 2017). Consequently, it is important to examine the influence of the addition of phase H ($MgSiO_4H_2$) to the stability of $CaCl_2$-type hydrous phases in the δ-AlOOH–ε-FeOOH phase H ternary system, which is expected to form over a wide composition range, and may carry a significant amount of hydrogen into the lower mantle.

Funding

This work was supported by JSPS KAKENHI Grant Numbers 18J12511 to C.X. and 26247073, 15H05828, 18H03740 to T.I. C.X. was supported by Research Fellowships of the Japan Society for the Promotion of Science (JSPS) for Young Scientists (DC2).

References cited

Bindi, L., Nishi, M., Tsuchiya, J., and Irifune, T. (2014) Crystal chemistry of dense hydrous magnesium silicates: The structure of phase H, $MgSiH_2O_4$, synthesized at 45 GPa and 1000 °C. American Mineralogist, 99, 1802–1805.

Bindi, L., Nishi, M., and Irifune, T. (2015) Partition of Al between Phase D and Phase H at high pressure: Results from a simultaneous structure refinement of the two phases coexisting in a unique grain. American Mineralogist, 100, 1637–1640.

Chang, Y.Y., Hsieh, W.P., Tan, E., and Chen, J. (2017) Hydration-reduced lattice thermal conductivity of olivine in Earth's upper mantle. Proceedings of the National Academy of Sciences, 114, 4078–4081.

Frost, D.J., and Fei, Y. (1998) Stability of phase D at high pressure and high temperature. Journal of Geophysical Research: Solid Earth, 103(B4), 7463–7474.

Fukuyama, K., Ohtani, E., Shibazaki, Y., Kagi, H., and Suzuki, A. (2017) Stability field of phase Egg, $AlSiO_3OH$ at high pressure and high temperature: possible water reservoir in mantle transition zone. Journal of Mineralogical and Petrological Sciences, 112, 31–35.

Hu, Q., Kim, D., Yang, W., Yang, L., Meng, M., Zhang, L., and Mao, H. (2016) FeO_2 and FeOOH under deep lower-mantle conditions and Earth's oxygen–hydrogen cycles. Nature, 534, 241–244.

Hwang, H., Seoung, D., Lee, Y., Liu, Z., Liermann, H., Cynn, H., Vogt, T., Kao, C., and Mao, H. (2017) A role for subducted super-hydrated kaolinite in Earth's deep water cycle. Nature Geoscience, 10, 947–953.

Inoue, T. (1994) Effect of water on melting phase relations and melt composition in the system Mg_2SiO_4-$MgSiO_3$-H_2O up to 15 GPa. Physics of the Earth and Planetary Interiors, 85, 237–263.

Kawazoe, T., Ohira, I., Ishii, T., Boffa Ballaran, T., McCammon, C., Suzuki, A., and Ohtani, E. (2017) Single crystal synthesis of δ-(Al,Fe)OOH. American Mineralogist, 102, 1953–1956.

Komabayashi, T., Hirose, K., Funakoshi, K., and Takafuji, N. (2005) Stability of phase A in antigorite (serpentine) composition determined by in situ X-ray pressure observations. Physics of the Earth & Planetary Interiors, 151, 276–289.

Komatsu, K., Sano-Furukawa, A., and Kagi, H. (2011) Effects of Mg and Si ions on the symmetry of δ-AlOOH. Physics and Chemistry of Minerals, 38, 727–733.

Kuribayashi, T., Sano-Furukawa, A., and Nagase, T. (2013) Observation of pressure-induced phase transition of δ-AlOOH by using single-crystal synchrotron X-ray diffraction method. Physics and Chemistry of Minerals, 41, 303–312.

Litasov, K., and Ohtani, E. (2003) Stability of various hydrous phases in CMAS pyrolite-H_2O system up to 25 GPa. Physics and Chemistry of Minerals, 30, 147–156.

Mashino, I., Murakami, M., and Ohtani, E. (2016) Sound velocities of δ–AlOOH up to core–mantle boundary pressures with implications for the seismic anomalies in the deep mantle. Journal of Geophysical Research: Solid Earth, 121(2), https://doi.org/10.1002/2015JB012477.

Myhill, R., Frost, D.J., and Novella, D. (2017) Hydrous melting and partitioning in and above the mantle transition zone: Insights from water-rich MgO-SiO_2-H_2O experiments. Geochimica et Cosmochimica Acta, 200, 408–421.

Nishi, M. (2015) Deep water cycle: Mantle hydration. Nature, 8, 9–10.

Nishi, M., Irifune, T., Tsuchiya, J., Tange, Y., Nishihara, Y., Fujino, K., and Higo, Y. (2014) Stability of hydrous silicate at high pressures and water transport to the deep lower mantle. Nature Geoscience, 7, 224–227.

Nishi, M., Kuwayama, Y., Tsuchiya, J., and Tsuchiya, T. (2017) The pyrite-type high-pressure form of FeOOH. Nature, 547, 205–208.

Ohira, I., Ohtani, E., Sakai, T., Miyahara, M., Hirao, N., Ohishi, Y., and Nishijima, M. (2014) Stability of a hydrous δ-phase, AlOOH–$MgSiO_2(OH)_2$, and a mechanism for water transport into the base of lower mantle. Earth and Planetary Science Letters, 401, 12–17.

Ohtani, E., Litasov, K., Suzuki, A., and Kondo, T. (2001) Stability field of new hydrous phase, δ-AlOOH, with implications for water transport into the deep mantle. Geophysical Research Letters, 28, 3991–3994.

Panero, W.R., and Caracas, R. (2017) Stability of phase H in the $MgSiO_4H_2$-AlOOH-SiO_2 system. Earth and Planetary Science Letters, 463, 171–177.

Panero, W.R., and Stixrude, L.P. (2004) Hydrogen incorporation in stishovite at high pressure and symmetric hydrogen bonding in δ-AlOOH. Earth and Planetary Science Letters, 221, 421–431.

Pearson, D.G., Brenker, F.E., and Nestola, F. et al. (2014) Hydrous mantle transition zone indicated by ringwoodite included within diamond. Nature, 507, 221–224.

Sano, A., Ohtani, E., Kubo, T., and Funakoshi, K. (2004) In situ X-ray observation of decomposition of hydrous aluminum silicate $AlSiO_3OH$ and aluminum oxide hydroxide δ-AlOOH at high pressure and temperature. Journal of Physics and Chemistry of Solids, 65, 1547–1554.

Sano, A., Ohtani, E., Kondo, T., Hirao, N., Sakai, T., Sata, N., Ohishi, Y., and Kikegawa, T. (2008) Aluminous hydrous mineral δ-AlOOH as a carrier of hydrogen into the core–mantle boundary. Geophysical Research Letters, 35, 3303.

Suzuki, A. (2010) High-pressure X-ray diffraction study of epsilon-FeOOH. Physics and Chemistry of Minerals, 37, 153–157.

Suzuki, A., Ohtani, E., and Kamada, T. (2000) A new hydrous phase δ-AlOOH synthesized at 21 GPa and 1000 °C. Physics and Chemistry of Minerals, 27, 689–693.

Thompson, E.C., Campbell, A.J., and Tsuchiya, J. (2017) Elasticity of ε-FeOOH: Seismic implications for Earth's lower mantle. Journal of Geophysical Research: Solid Earth, 122, doi:10.1002/2017JB014168.

Tschauner, O., Huang, S., Greenberg, E., Prakapenka, V., Ma, C., Rossman, G., Shen, A., Zhang, D., Newville, M., Lanzirotti, A., and Tait, K. (2018) Ice-VII inclusions in diamonds: Evidence for aqueous fluid in Earth's deep mantle. Science, 359, 1136–1139.

Tsuchiya, J., and Tsuchiya, T. (2011) First-principles prediction of a high-pressure hydrous phase of AlOOH. Physical Review B, 83, 210–216.

Tsuchiya, J., Tsuchiya, T., and Tsuneyuki, S. (2002) First principles calculation of a high-pressure hydrous phase, δ–AlOOH. Geophysical Research Letters, 29, 15–11.

Walter, M.J., Thomson, A.R., Wang, W., Lord, O.T., Ross, J., McMahon, S.C., Baron, M.A., Melekhova, E., Kleppe, A.K., and Kohn, S.C. (2015) The stability of hydrous silicates in Earth's lower mantle: Experimental constraints from the systems MgO-SiO_2-H_2O and MgO-Al_2O_3-SiO_2-H_2O. Chemical Geology, 418, 16–29.

Wirth, R., Vollmer, C., Brenker, F., Matsyuk, S., and Kaminsky, F. (2007) Inclusions of nanocrystalline hydrous aluminium silicate "Phase Egg" in superdeep diamonds from Juina (Mato Grosso State, Brazil). Earth and Planetary Science Letters, 259, 384–399.

Xue, X., and Kanzaki, M. (2007) High-pressure δ-$Al(OH)_3$ and δ-AlOOH phases and isostructural hydroxides/oxyhydroxides: New structural insights from high-resolution ^1H and ^{27}Al NMR. Journal of Physical Chemistry B, 111, 13156–13166.

Zhong, X., Hermann, A., Wang, Y., and Ma, Y. (2016) Monoclinic high-pressure polymorph of AlOOH predicted from first principles. Physical Review B, 94(22), 224110.

Manuscript received March 25, 2019
Manuscript accepted June 14, 2019
Manuscript handled by Ryosuke Sinmyo